

IET Renewable Power Generation

Special Issue Call for Papers

**Be Seen. Be Cited.
Submit your work to a new
IET special issue**

Connect with researchers and
experts in your field and
share knowledge.

Be part of the latest research
trends, faster.

[Read more](#)



The Institution of
Engineering and Technology

ORIGINAL RESEARCH

Concurrent frequency–voltage stabilization for hybrid microgrid with virtual inertia support

Abdul Latif¹ | S. M. Suhail Hussain^{2,3}  | Atif Iqbal⁴  | Dulal Chandra Das⁵ |
Taha Selim Ustun⁶ | Ahmed Al-Durra¹

¹Advanced Power and Energy Center, EECS Department, Khalifa University, Abu Dhabi, United Arab Emirates

²Electrical Engineering Department, King Fahd University of Petroleum and Minerals (KFUPM), Dhahran, Saudi Arabia

³Interdisciplinary Research Center for Renewable Energy and Power Systems (IRC-REPS), King Fahd University of Petroleum and Minerals (KFUPM), Dhahran, Saudi Arabia

⁴Department of Electrical Engineering, Qatar University, Doha, Qatar

⁵Department of Electrical Engineering, National Institute of Technology Silchar, Assam, India

⁶Fukushima Renewable Energy Institute, AIST (FREI), Koriyama, Japan

Correspondence

Atif Iqbal, Department of Electrical Engineering, Qatar University, Doha, Qatar.
Email: atif.iqbal@qu.edu.qa

Funding information

Khalifa University, Grant/Award Number: KAU-KU-2021-01; Qatar National Library (QNL); Khalifa University, Grant/Award Number: KAU-KU-2021-01

Abstract

This paper presents a novel control scheme for combined frequency and voltage stabilization of an islanded multi-generator hybrid microgrid (IH μ G). The control concept incorporates an improved virtual inertia support scheme (IVIS) and the recently developed yellow saddle goatfish technique (YSGA) to obtain optimal control parameters. IH μ G model consists of an AVR-based voltage compensating loop for synchronous biodiesel generator, wind generator, wave generator, photon exchange membrane fuel cell (PEMFC), and controllable heat pump and freezer. An integer order proportional-integral-derivative (IOPID) controller is leveraged for frequency-voltage stabilization. A comparative response assessment has been performed with/without IVIS. The utilization of YSGA has been justified by comparative assessment with particle swarm optimization, firefly, and sine-cosine techniques. A meticulous performance evaluation of YSGA optimized IOPID control scheme in the IH μ G has been conducted through several case studies. Furthermore, the rigorous sturdiness assessment of YSGA optimized IOPID controller was performed under different uncertainties such as: variation of amplifier gain, $\pm 30\%$ variation in demanded loading magnitude, moment of inertia and droop coefficient. Finally, real-time hardware-in-the-loop (HIL) simulation platform is utilized to validate the proposed control approach.

1 | INTRODUCTION

Strategic energy policies require energy management solutions in modern microgrids with lesser environmental impact and carbon footprint [1–3]. The massive penetration of renewable resources (RRs) and the exaggerated load demands could affect the stable operation system [4]. The intermittent nature of RRs may cause voltage and frequency issues. Therefore, in renewable energy-dominated microgrids with low-inertia, a proper control scheme is required [5].

Recently, numerous researchers have attempted to suppress frequency and voltage deviations in hybrid microgrids [6–11]. In [6] wind-solar thermal energy-based frequency sensitive

microgrid power system is analysed. Where battery and ultra-capacitor are the indispensable units to solve the problem. Li et al. [7] demonstrate a primary frequency stabilization using hybrid battery and super magnetic storage units. The multi-renewable energy (wind-PV)-diesel-storages units (i.e. battery, flywheel) utilized in two-area frequency response microgrid system is addressed in [8], whereas the system stability assessment in accordance with voltage is analysed in [9]. Zhu et al. [10] discussed the coordination of renewable energy sources with electric vehicle for improving the frequency responses of isolated microgrid. In order to level the power fluctuation smoother the application thermostatically controllable loads for frequency response isolated power system is investigated in [11].

This is an open access article under the terms of the [Creative Commons Attribution](https://creativecommons.org/licenses/by/4.0/) License, which permits use, distribution and reproduction in any medium, provided the original work is properly cited.

© 2023 The Authors. *IET Renewable Power Generation* published by John Wiley & Sons Ltd on behalf of The Institution of Engineering and Technology.

The study of literature shows that they only focus on separate frequency and voltage stabilization issue with consideration of conventional diesel and battery, ultracapacitor and flywheel storage units. So, the eco-friendly biodiesel power generator can be a potential alternative to a diesel unit. Nonetheless, maintenance and dumping issues of battery, slow response of flywheel units and expensive helium liquid in supermagnetic storage units bottleneck their contribution in frequency regulation of microgrid power system. In this regard, a newly developed environment friendly fuel cell named photon exchange membrane fuel cell (PEMFC) gain much interest to be a part of microgrid system which not yet explored. Very few articles have considered the voltage stabilization along with frequency stabilization issue for the large-scale conventional power network [12–14]. Work in [12] has proven the efficacy of damping based automatic load frequency control (ALFC) and automatic voltage regulator (AVR) scheme to improve the system dynamics. Whereas [13, 14] have deliberated the effect of ALFC and AVR in the dynamic responses (frequency and voltage) for large scale interconnected power model.

However, less attention has been paid to designing coordinated control strategies for concurrent frequency and voltage stabilization of islanded renewable microgrid system. In fact, frequency and voltage instability are two major phenomena that may cause microgrid instability leading to power blackouts. In order to improve the inertia in microgrid virtual inertia support (VIS) scheme has been used [15–18]. As such few articles have considered controllable derivative technique-based VIS scheme in recent time using ultracapacitor unit for frequency regulation of power network [16–24]. The frequency stability of the high voltage DC-linked system was improved in [16–18] by applying the derivative method-based inertia control. Sockeel et al. [25] suggested controlling the inertia power using a derivative technique using model predictive control. Fang et al. [26] recently investigated enhancement of inertia based on frequency derivatives while taking frequency measurement into account. However, the majority of the published research work in this field [16–25] ignores the design of virtual damping, which is crucial in giving the microgrids extra damping properties. The absence of virtual damping may cause virtual inertia control to operate insufficiently in low inertia-damping based microgrid system. In the case of a poor load-damping factor of the microgrid during low power consumption, this would may amplified, leading to system instability and collapse [20].

Therefore, Bevrani et al. [15] developed a detailed outline of virtual synchronous generator (VSG) for islanded power systems with distributed generation. This model is improved in [27] to enhance the transient stability of large-scale power networks. In order to damp the oscillation, energy storage unit (ESU) based VSG is utilized [28]. Furthermore, very less attention has been given in the literature on improving voltage stability using VIS technique. In that direction modelling of derivative technique-based virtual inertia support (IVIS) is crucial to improve system damping, inertia, and frequency as well as voltage stability. Considering the importance of power quality of islanded multi-generator hybrid microgrid (IH μ G), the concurrent frequency and voltage stabilization with IVIS scheme

can be considered. This can be incorporated with automatic microgrid load frequency control (A μ LFC) and voltage restorer (A μ VVR). This has the potential to improve both the frequency and voltage behaviour of IH μ Gs and has not been explored in the literature yet.

In the deep concentration on the problem related to frequency and voltage regulation analysis, the optimal adjustment of the controller is interrelated to improve the change in output power of different subsystems associated with the load frequency controller and voltage controller responding to concurrent frequency-voltage stabilization based on certain algorithm. Recently, several controllers have been used to solve the load frequency stabilization problem. The efficacy of the classical proportional-integral-derivative (CPID) controller over other classical proportional-integral (CPI), classical proportional-derivative (CPD) and classical integral-derivative (CID) are explored for frequency response in microgrids [6, 29–31]. In addition, some other controllers such as integer, non-integer PID [32, 33] and model predictive controllers [34] have been collaborated with PID for similar kinds of frequency regulation. Therefore, the proposed work is motivated to utilize integer-order PID (IOPID) for the proposed frequency-voltage stabilization of IH μ G.

Additionally, the use of several optimization techniques to improve the system dynamics is vital. Applications of different techniques for obtaining control parameters pertinent to dynamic response stabilization of conventional/microgrid power networks have been surveyed in [35]. Genetic technique (GA) [6], particle swarm optimization (PSO) [32], firefly [33], improved JAYA technique (IJAYA) [8], flower pollination technique (FPA) [9], social-spider approach (SSO) [31], sine-cosine technique (SCA) [36], imperialist competitive technique (ICA) [37], grasshopper technique (GOA) [38]. Furthermore, according to no-free-lunch (NFL) theory, no algorithm can solve all optimization problems. Thus, applying powerful meta-heuristic techniques for obtaining optimum solutions is always open to improve the balance between exploration and exploitation phases. Unlike other meta-heuristic techniques, a recently established bio-inspired approach called the yellow saddle goatfish technique (YSGA) [39] promises better optimization performance to balance exploration and exploitation phases. The advantages of YSGA over other algorithmic tools are that it offers accuracy, higher exploration-exploitation which leads to higher convergence characteristics. Therefore, the present work measures the computational ability of YSGA for shaping the system performance. This helps to find a feasible solution to make the IVIS more useful in microgrid power system. A comparison with other similar comparable existing approaches is included in Table 1 which further emphasizes the contribution of the proposed coordinated control method. Comparatively, the proposed approach offers the advantages of joint improvement for concurrent frequency-voltage stability and dynamic performance. Considering the above discussion, this work is motivated by the following attributes:

- a. Due to rapid depletion of fossil fuel resources, and global warming effects, a reliable and well-controlled hybrid

TABLE 1 Review summary of similar existing method for regulating dynamic responses in power system

| Ref. no. | System components | RRs | Frequency/voltage regulation | Virtual inertia support | System stability analysis | Convergence analysis of optimization |
|----------|---|-----|------------------------------|-----------------------------|---------------------------|--------------------------------------|
| [16] | Conventional generations | * | Only frequency | √ | √ | * |
| [17] | Conventional generations | * | Only frequency | √ (only virtual inertia) | √ | * |
| [18] | Conventional generations | * | Only frequency | √ (only virtual inertia) | √ | * |
| [19] | Thermal, wind, solar | √ | Only frequency | √ (only virtual inertia) | √ | * |
| [20] | Solar, wind, diesel | √ | Only frequency | √ (only virtual inertia) | * | * |
| [21] | Thermal, wind | √ | Only frequency | √ (only virtual inertia) | * | * |
| [25] | Thermal, wind, solar | √ | Only frequency | √ (only virtual inertia) | * | * |
| [23] | Thermal, wind, solar | √ | Only frequency | √ (only virtual inertia) | √ | * |
| [24] | Thermal, wind, solar | √ | Only frequency | √ (only virtual inertia) | √ | * |
| [37] | Wind, solar PV, diesel | √ | Only frequency | * | * | √ |
| Proposed | Wind, wave, biodiesel, photon exchange membrane fuel cell, non-critical loads | √ | Both frequency and voltage | Virtual inertia and damping | √ | √ |

microgrid housing renewable-bio energy sources have gained significant attention.

- b. Due to the high penetration of RRs and dramatic variation in load demand in low-inertia microgrid system, the design of the virtual inertia support for frequency-voltage response is indispensable.
- c. Although different controllers reported in literature improve performance, the dynamic response (i.e. frequency and voltage) under real-time scenario is still to be explored.
- d. NFL theory encourages researchers to explore and apply powerful meta-heuristic techniques for searching better near-optimum design parameters of frequency as well as voltage controllers.

The significant contributions of the proposed work are summarized below:

- a. To develop a maiden islanded multi-generator hybrid microgrid (IH μ G) that consists of wind driven generation (WDG), wave driven power generation (WVPG), bio-diesel power generation (BDG), photon exchange membrane fuel cell (PEMFC), controllable heat pump (CHP) and freezer (CFRZ).
- b. To design of novel improved virtual inertia support (IVIS) scheme and its utilization for concurrent frequency-voltage stabilization of the proposed renewable energy based microgrid.
- c. To establish the modelling of PEMFC unit in proposed frequency-voltage response IH μ G system.
- d. To select best controller and optimization technique among PI, ID, IPD, IOPID and PSO, FA, SCA, YSGA for optimal frequency as well as voltage responses of the proposed IH μ G.
- e. To evaluate the system dynamics under concurrent non-linear real-recorded wind data, wave and load pattern.

- f. To assess the influence of improve virtual inertia scheme in system dynamics (frequency and voltage characteristics) and compare a stability analysis of proposed control technique with IVIS against without IVIS.
- g. To evaluate the sturdiness of the proposed approach the system undergoes a sensitivity test under different parametric variations and uncertain conditions.
- h. To validate of the proposed control approach using OPAL-RT real-time computing platform under hardware-in-the-loop (HIL) environment and compare the dynamic response with and without OPAL-RT results.

The above said points have been the encouraging aspects of this research. The rest of the paper is organized as follows: Section 2 presents the proposed IVIS and dynamic model of the studied microgrid. Sections 3 and 4 reveal the overview of YSGA technique and methodology, while Section 5 presents simulations, tests and discussion of results. Finally, Section 6 draws conclusions.

2 | DESIGN OF DYNAMIC MODEL OF MICROGRID AND THE PROPOSED IVIS

The modelling of proposed microgrids' system components are the first step towards implementation of the work. In order to analyse the system dynamics, the modelling of proposed microgrid comprising of wind driven generation (WDG), wave driven power generation (WVPG), bio-diesel power generation (BDG), photon exchange membrane fuel cell (PEMFC), controllable heat pump (CHP) and freezer (CFRZ) has been done and is presented in Figure 1a. The mathematical modelling of WDG, WVPG, BDG, CHP and CFRZ has been reported in [40–42]. The proposed microgrid model encompassed a maiden IVIS control design with $A\mu$ VR control loop. The set

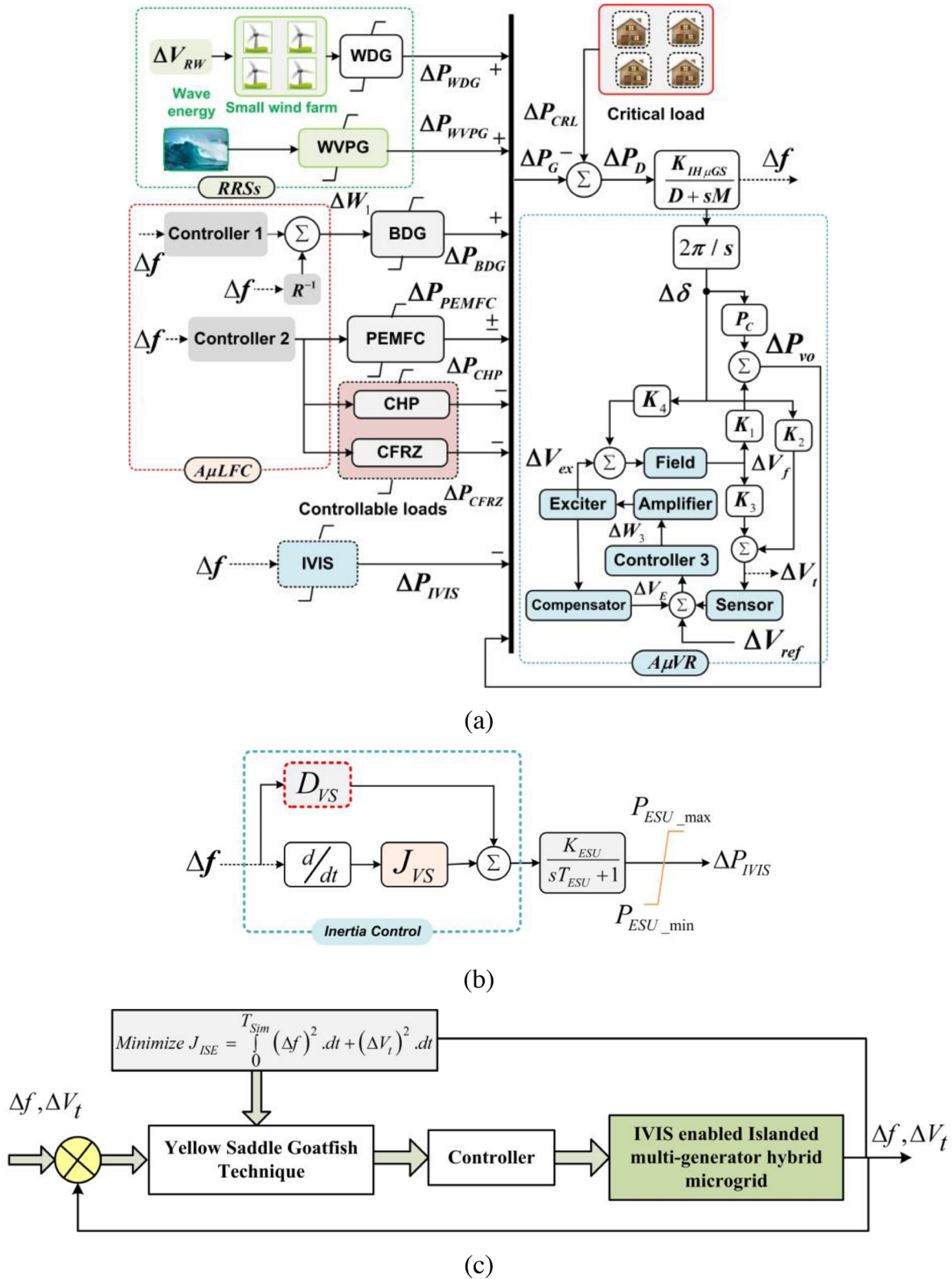


FIGURE 1 (a) Proposed schematics of IVIS employed dual-area I μ PS, (b) Representation of proposed IVIS scheme, (c) flow diagram of controller tuning process for I μ PS.

TABLE 2 Nomenclature with symbols with values

| Nomenclature | | Value |
|--|--|-------------------------------|
| $\Delta f, \Delta V_t$ | Frequency fluctuation and change in terminal voltage of IH μ G | – |
| $K_{IH\mu G}$ | Gain of IH μ G system | 1 |
| ΔP_G | Total change in generated power | – |
| $\Delta P_{CRL}, \Delta P_D, \Delta P_{IVS}$ | Change of power of critical load, net power deviation and improved virtual inertia support | – |
| ΔP_{VO} | Power variation of A μ VR loop | – |
| K_{WDG}, T_{WDG} | WDG system gain and time values | 1, 1.5 s |
| K_{WVPG}, T_{WVPG} | Gain and time values of WVPG | 1, 0.3 s |
| K_{VR}, K_{CE} | Gains' of valve positioner and internal combustion engine of BDG | 1, 1 |
| T_{VR}, T_{CE} | Time constants' of valve positioner and internal combustion engine of BDG | 0.05 s, 0.5 s |
| K_{CHP}, T_{CHP} | Gain and time value of CHP | 1, 0.1 s |
| K_{CFRZ}, T_{CFRZ} | Gain and time value of CFRZ | 1, 0.2465 s |
| J_{VS}, D_{VS} | Virtual inertia and damping values of IVIS | 1.6, 1.2 |
| K_{ESU}, T_{ESU} | Gain and inverter enabled time constant of ESU | 1, 0.2 s |
| $P_C, K_1, K_2, K_3, \text{ and } K_4$ | Coupling co-factors of A μ VR | 0.145, 0.2, –0.1, 0.5 and 1.4 |
| K_a, T_a | Gain and time value of amplifier | 10, 0.1 s |
| K_e, T_e | Gain and time value of exciter | 1, 0.4 s |
| K_f, T_f | Gain and time value of field | 0.8, 1.4 s |
| K_s, T_s | Gain and time value of sensor | 1, 0.05 s |
| K_{cm}, T_{cm} | Gain and time value of compensator | 0.5, 0.715 s |
| R | Constant droop values of IH μ G | 0.05 |
| M | IH μ GS moment of inertia | 0.12 s |
| D | Damping factor of IH μ GS | 0.1 (p.u./Hz) |
| V_{RW} | Intermittent wind velocity | – |
| V_{cut-in} | Cut-in velocity of wind to drive the WDG | – |
| V_{rated} | Nominal wind velocity | – |
| $V_{cut-out}$ | Cut-out velocity of wind to stop the WDG | – |
| $NIWE$ | National Institute of Wind Energy (India Government) | – |
| $Iter_{Max}$ | Maximum iterations | 100 |

of considered parameters with gain, time constants, and other control parameters are given in the Table 2.

2.1 | Wind driven generation (WDG)

The intermittent nature wind driven power is produced by wind turbine through mechanical to electrical power conversion. That extractable wind power is very much dependent on wind velocity and other inherent identification of wind turbine. The first stage mechanical power from wind velocity can be expressed as [32];

$$P_{WD} = 0.5\rho \times V_{WD}^3 \times S_b \times C_p(\lambda, \beta) \quad (1)$$

where ρ , V_{WD} , S_b , and C_p are the air density, intermittent wind velocity, turbine's blade swept area and the extractable power coefficient respectively. The expression of C_p could be illustrated

as

$$10C_p = 5.17 \left(\frac{1160}{\lambda + 0.08\beta} - \frac{40.6}{1 + \beta} - 0.8\beta - 50 \right) e^{\left(-\frac{21}{\lambda}\right)} + 0.068\lambda \quad (2)$$

The internal function λ and β are the tip-speed ratio and blade pitch angle respectively. A real-time recorded datasheet (provided by National Institute of Wind Energy, India) of Akkanayakanpatti wind power station is considered in this work as shown in the Appendix. The rate of change of considered station's wind power generation with its complete transfer function model could be represented as below [40].

$$P_{WDG} = \begin{cases} 0, & V_{WD} < V_{cut-in} \parallel V_{WD} > V_{cut-out} \\ P_{rated}, & V_{rated} \leq V_{WD} \leq V_{cut-out} \\ \left(0.001312V_{WD}^6 - 0.04603V_{WD}^5 - 0.3314V_{WD}^4 \right. \\ \left. + 3.687V_{WD}^3 - 51.1V_{WD}^2 + 2.33V_{WD} + 366 \right), & \text{else} \end{cases} \quad (3)$$

$$\Delta P_{WDG} = \begin{cases} 0, & V_{WD} < V_{cut-in} \parallel V_{WD} > V_{cut-out} \\ 0, & V_{rated} \leq V_{WD} \leq V_{cut-out} \\ \left(\begin{aligned} & \left[0.007872V_{WD}^5 - 0.23015V_{WD}^4 - 1.325V_{WD}^3 \right. \\ & \left. + 11.061V_{WD}^2 - 102.2V_{WD} + 2.33 \right] \Delta V_{WD} \end{aligned} \right), & else \end{cases} \quad (4)$$

where $G_{WDG}(s) = \frac{K_{WDG}}{T_{WDG}s+1}$

2.2 | Wave driven power generation (WVPG)

To generate the power from wave energy a permanent magnet synchronous generator (PMSG) is leveraged. The active speed and force to extract power from WVPG could be expressed as [41],

$$v_{FG} = \frac{dx}{dt} \quad (5)$$

$$F_{WV} = m_{\beta} \frac{dv_{FG}}{dt} + \beta_G v_{FG} + \beta_{\omega} v_{FG} + k_C x \quad (6)$$

where v_{FG} and F_{WV} are the velocity (m/s) of the floater-generator set and wave strengths (N) respectively. The m_{β} is the overall mass in (kg). Corresponding to Equation (6) the non-linear sinusoidal wave force could be formulated as

$$F_{WV} = F \sin(\omega_{WV}t) + \frac{F}{2} \sin(2\omega_{WV}t) + \frac{F}{3} \sin(3\omega_{WV}t) \quad (7)$$

The linearized transfer function of WVPG can be deliberated as [41],

$$G_{WVPG}(s) = \frac{K_{WVPG}}{T_{WVPG}s+1} \quad (8)$$

2.3 | Bio-diesel generation (BDG)

The biodegradable, high efficacy-based power generation from non-toxic BDG is independently proficient of delivering the deficiency of power and could be minimize the power mismatch between generation and demand. The linearized model of BDG could be formed as,

$$\Delta W_{MBG} = W(s) - (R^{-1} \times \Delta f) \quad (9)$$

$$\Delta P_{VR} = \Delta W_{BDG} - (R^{-1} \times \Delta f) \quad (10)$$

$$\Delta P_{GCE} = \Delta P_{VR} \times \left(\frac{K_{VR}}{T_{VR}s+1} \right) \quad (11)$$

$$\Delta P_{BDG} = \Delta P_{GCE} \times \left(\frac{K_{CE}}{T_{CE}s+1} \right) \quad (12)$$

where ΔW_{BDG} and $W(s)$ are the change in input error of BDG and the output control signal of the controller.

2.4 | Photon exchange membrane fuel cell (PEMFC)

The PEMFC transforms concentrated chemical energy into electricity. The lower temperature ($\approx 80-100^\circ\text{C}$) and faster response time are the motivating factors to choose PEMFC unit among other FC units. With considering the mass flow rate (Q_{H_2}) and pressure (P_{H_2}) the PEMFC can be mathematically modelled by,

$$\frac{Q_{H_2}}{P_{H_2}} = \frac{K_{ad}}{\sqrt{M_{H_2}}} \quad (13)$$

With extending, the partial pressure of hydrogen could be formulated as;

$$P_{H_2} \frac{d}{dt} = \left(\frac{1}{V_{ad}} \right) RT \left(Q_{H_2}^{ipt} - Q_{H_2}^{opt} - Q_{H_2}^f \right) \quad (14)$$

$$Q_{H_2}^r = \left(\frac{1}{2F} \right) N_0 N_s I_{fc} = 2K_r I_{fc} \quad (15)$$

$$P_{H_2} = \frac{(K_{H_2})^{-1}}{1 + \left(\frac{V_{ad}}{K_{H_2}RT} \right) \cdot s} \left(Q_{H_2}^{ipt} - 2K_r I_{fc} \right) \quad (16)$$

The output cell voltage of PEMFC could be formulated as

$$V_{OS} = E_c - Bln(CI_{fc}) - R^{int} I_{fc} \quad (17)$$

where E_c is the controlled voltage.

$$E_c = N_0 \left\{ E_0 + \left(\frac{1}{2F} \right) RT \log \left(\frac{P_{H_2} \times \sqrt{P_{O_2}}}{P_{H_2^0}} \right) \right\} \quad (18)$$

The detail specification of the system parameters are discussed in [42].

2.5 | Controllable loads

The controllable heat pump (CHP) and freezer (CFRZ) loads are used in the proposed work for smoother power management as well as to improve the system dynamics. The first order CHP and CFRZ model are adopted here as follows [43]

$$G_{CHP}(s) = \frac{K_{CHP}}{T_{CHP}s + 1} \quad (19)$$

$$G_{CFRZ}(s) = \frac{K_{CFRZ}}{T_{CFRZ}s + 1} \quad (20)$$

2.6 | Automatic microgrid frequency restorer (AμFR)

The AμFR can be model according to the schematic proposed diagram. The equations that illustrated this phenomenon is formulated by Equation (21),

$$\Delta W_i = \left\{ (\text{Transfer function of controller}) - R^{-1} \right\} \times \Delta f \quad (21)$$

$$\Delta W_i = (\text{Transfer function of controller}) \times \Delta f \quad (22)$$

where $i = 1, 2$. The combined effect of controller's control signal and error signal of microgrid is represented as ΔW .

2.7 | Modelling of improved virtual inertia support (IVIS) scheme

The penetration of non-synchronous generator-enabled renewable resources in the microgrid power network is the driving force for the future carbon-neutral society. Hence the power converter coupled non-synchronous generators reduce the inertia (M) of the whole power network and provide higher frequency fluctuation problem. To mitigate such issue, conventional virtual inertia support (VIS) concept has been implemented. Here, an improved virtual inertia support (IVIS) technique considering virtual damping (D_{VIS}) and virtual inertia has been modelled to enhance system dynamics. To establish this concept, short term converter coupled energy storage unit (ESU) is required with suitable inertia control.

Hence, some recent works [19, 20] have utilized ultracapacitor based conventional VIS scheme to manage the active and reactive power for higher inertia traditional power network. However, the IVIS is not yet explored. The proposed work established the maiden IVIS scheme considering the hEV ESU.

The designed control scheme is applied to operate as an independent control unit and will enhance the system dynamics frequency and voltage stabilization. The designed IVIS scheme is framed in Figure 1b. The illustration of the derivative technique (d/dt) is leveraged to determine the change in frequency during uncertainty conditions. Moreover, to stabilize the system dynamics with a faster time frame, virtual damping (D_{VIS}) is leveraged. As a result, the change in virtual damping-inertia supported power will improve the system dynamic responses as compared to conventional VIS approach. Considering the above said features, the proposed control mechanism could be depicted as

$$\Delta P_{IVIS} = (J_{VIS}s + D_{VIS}) \times \left\{ \frac{K_{ESU}}{sT_{ESU} + 1} \right\} \times \left[\frac{d(\Delta f)}{dt} \right] \quad (23)$$

The considered system parameters are displayed in Table 2.

2.8 | Automatic microgrid voltage restorer (AμVR)

To realize the effect of voltage excitation system an AμVR loop is employed with the generator of the BDG in the proposed microgrid model. The IEEE type-1 excitation loop consists of exciter, amplifier, compensator, field, sensor and a controller. The controller action could be expressed by Equation (24).

$$\Delta W_3 = (\text{Transfer function of controller}) \times \Delta V_E \quad (24)$$

The different control actions for voltage regulation in AμVR loop such as; power variation (ΔP_{vo}), terminal voltage change (ΔV_t), error signal (ΔV_E), field voltage (ΔV_f) and change in exciter voltage (ΔV_{ex}) are expressed by Equations (25)–(29) respectively [44].

$$\Delta P_{vo} = P_c \Delta \delta + K_1 \times \Delta V_f \quad (25)$$

$$\Delta V_t = K_2 \Delta \delta + K_3 \times \Delta V_f \quad (26)$$

$$\Delta V_f = \left(\frac{K_f}{sT_f + 1} \right) \times (\Delta V_{ex} - K_4 \times \Delta \delta) \quad (27)$$

$$\Delta V_E = \Delta V_{ref} - \left(\frac{K_{cm}}{sT_{cm} + 1} \right) \times \Delta V_{ex} - \left(\frac{K_s}{sT_s + 1} \right) \times \Delta V_t \quad (28)$$

$$\Delta V_{ex} = \Delta W_3 \times \left(\frac{K_a}{sT_a + 1} \right) \times \left(\frac{K_e}{sT_e + 1} \right) \quad (29)$$

where P_c is the synchronising power constant.

2.9 | Overall system dynamic model

Considering all the subsystems' power in the proposed IHμG, the dynamic load-generator model could be obtained as follows;

$$\Delta f = \left(\frac{K_{IH\mu GS}}{sM + D} \right) \times \Delta P_G \quad (30)$$

$$\begin{aligned} \Delta P_G = (\Delta P_{RRS} + \Delta P_{BDG} \pm \Delta P_{PEMFC} \\ - \Delta P_{CHP} - \Delta P_{CRFZ} = \Delta P_{CRL} \rightarrow 0) \end{aligned} \quad (31)$$

$$\Delta P_D = \Delta P_G \pm \Delta P_{TVS} \pm \Delta P_{v0} - \Delta P_{CRL} \quad (32)$$

The specified values of the system parameters are displayed in Table 2.

3 | OVERVIEW OF YELLOW SADDLE GOATFISH TECHNIQUE

In recent time, in 2018, Zaldiver et al. proposed a bio-stimulated saddle of yellow goatfish evolutionary technique (YSGA). The YSGA simulates group hunting action of yellow goatfish (*Parupeneus cyclostomus*) [39]. The details of YSGA technique is described in [39]. The concept of hunting process of yellow goatfish could be constructed in five essential stages namely; initialization, chasing, blocking, role exchange and zone change.

3.1 | Stage 1: Initialization

This stage starts with a population of K of x (search agents) goatfish is dispersed (K_1, K_2, \dots, K_x) in the search plane 'y'. The initialization could be written as

$$\begin{aligned} K_i^j = rand \times (B_j^{max} - B_j^{min}) + B_j^{min} \text{ i.e. } i \\ = 1, 2, \dots, x \text{ and } j = 1, 2, \dots, y \end{aligned} \quad (33)$$

B_j^{max} and B_j^{min} are the limits of the boundary. The main goals of this stage are to establish a supportive search by assembling a cluster among the neighbourhood. The detection and separation process among search agents and number of clusters (C) are framed in [39].

3.2 | Stage 2: Chasing

Based on the superior fitness solution, every C chooses a γ_F chasing fish in the K th population to construct the predator. To trap the hided prey, sometime γ_F will shift from its last position which could be formulated as

$$\gamma_F^{t+1} = \gamma_F^t + \alpha \oplus Levy(\mu) \text{ i.e. } 0 < \mu \leq 2 \quad (34)$$

where α, μ state the step size of onlooker γ_F and levy mutation index. To establish the superior predation, the performance of each cluster set could be written as

$$R_s = \alpha \oplus Levy(\mu) \sim \alpha \left(\frac{U}{|V|^{\frac{1}{\beta}}} \right) (\gamma_F^t - \gamma_{Fbest}^t) \quad (35)$$

where R_s, γ_{Fbest}^t states the random step and superior γ_F among all the clusters. The dissemination U and V is presented in [39]. The trapping activity is progressed with a new position of γ_F and γ_H can be formulated as

$$\gamma_F^{t+1} = \gamma_F^t + R_s \quad (36)$$

$$\gamma_{Fbest}^{t+1} = \gamma_{Fbest}^t + R_s^t \quad (37)$$

3.3 | Stage 3: Blocking

In order to catch the prey, the construction of trapping (i.e. blocking) could be formed by choosing chaser fish from each cluster, where the remaining fishes are blocker fish (γ_H) as shown in [39]. The position updating equation of γ_H could be calculated based on the logarithmic spiral written as

$$\gamma_H^{t+1} = D_f \times e^{b\rho} \times \cos 2\pi\rho + \gamma_F \quad (38)$$

where ρ states the (closeness in between chaser and blocker fish) the randomly generated number among $(a, 1)$. D_f is the distance that states the current positional difference between γ_F and γ_H as in [39].

3.4 | Stage 4: Role change

In this stage, the initial assumption states the superior fitness solution among any 'C' is γ_F . In this regard, the hunting process follows the above said behaviour by which the prey move towards the hunting zone. As a result, the closer movement of γ_H to achieve the prey developed a new γ_F .

3.5 | Stage 5: Zone change

In this procedure, after catching all the prey from a cluster the zone changing process occur to find the new prey. During the procedure, the overexploitation parameter (λ) is incorporated. So, the formation of zone change equation of YSGA could be stated as follows:

$$s_{gf}^{t+1} = \frac{\gamma_{Fbest} + s_{gf}^t}{2} \quad (39)$$

where s_{gf}^{t+1} states the newly developed goatfish location. γ_{Fbest} is the superior result among all the cluster groups determined by ' γ_F '. The specification of YSGA techniques is depicted in Appendix.

TABLE 3 Different controllers tuned parameters

| Control scheme | PI | ID | IPD | IOPID |
|----------------|-------|-------|-------|-------|
| K_{P1} | 14.07 | – | 8.01 | 40.68 |
| K_{I1} | 49.95 | 11.45 | 37.25 | 26.84 |
| K_{D1} | – | 16.83 | 29.70 | 2.47 |
| K_{P2} | 50.63 | – | 50.24 | 45.03 |
| K_{I2} | 10.26 | 50.07 | 49.27 | 27.22 |
| K_{D2} | – | 49.47 | 51.09 | 24.89 |
| K_{P3} | 1.95 | – | 5.48 | 4.97 |
| K_{I3} | 0.14 | 8.51 | 17.60 | 21.24 |
| K_{D3} | – | 3.46 | 4.33 | 4.62 |

TABLE 4 Analysed result of different controller

| Controllers | | PI | ID | IPD | IOPID |
|----------------------------|--------------|------------------------|------------------------|------------------------|------------------------|
| J_{min} | | 1.188×10^{-5} | 1.516×10^{-5} | 5.101×10^{-7} | 2.093×10^{-7} |
| $+O_{vs} (\times 10^{-4})$ | Δf | 62.96 | 7.57 | 0.89 | 0.076 |
| | ΔV_i | 0.89 | 2.76 | 0.48 | 0.28 |
| $-U_{vs} (\times 10^{-4})$ | Δf | 90.66 | 7.84 | 5.46 | 0.014 |
| | ΔV_i | 9.58 | 2.59 | 5.87 | 4.93 |
| $T_{st} (s)$ | Δf | 12.41 | Unsettle | 11.09 | 8.89 |
| | ΔV_i | 8.90 | Unsettle | 8.73 | 3.14 |

3.6 | Computational burden of YSGA

The considered microgrid system consists of multiple coupled subsystems. A linearized mathematical model will be especially useful in creating the control algorithm and reduce the computation burden associated with its optimization technique. In optimization, the burden of computation is determined by a relation between the calculation time and the issue size. Therefore, the Big-C symbol is used here as a common phrasing. The burden is depends on the number of particles or search agent (n), the quantity of dimensions (d), number of generation or iterations (i) and the expense of function evaluation (c).

$$\begin{aligned}
C(YSGA) = & C(\text{problem de fination}) + C(\text{initilization}) \\
& + C\{i(\text{function evaluations})\} \\
& + C\{i(\text{memory saving})\} \\
& + C\{i(\text{position update})\} \quad (40)
\end{aligned}$$

As a result, the overall computational burden can be calculated as follows:

$$C(YSGA) = C(1 + nd + icn + in + ind) \cong C(ind + icn) \quad (41)$$

As it has been demonstrated, the burden is polynomial in nature. YSGA can therefore be considered as a productive algorithm. Similarly, the computational burden of considered PSO, FA and SCA can be calculated.

4 | STRATAGEM OF METHODOLOGY

4.1 | Objective problem formulation and constraints

In order to reach an optimum solution, utilization of appropriate objective function is an important task. To achieve the abovementioned objective an integral square error (ISE) is illustrated in (42).

$$\text{Minimize } J_{ISE} = \int_0^{T_{sim}} (\Delta f)^2 dt + (\Delta V_i)^2 dt \quad (42)$$

To get a better dynamic response of the given low inertia microgrid, the optimal coordinated control between virtual inertia and load frequency controller using optimization technique is important. In this study, an integer order proportional (P)-integral (I)-derivative (D) (IOPID) controller is leveraged which is the most effective option because it is easy to structure, has a genuine and perfect execution, and comes at an affordable price. In the selected microgrid system, the three IOPID controllers are tuned by an intelligent searching technique named YSGA technique. The transfer function of the IOPID controller $G_{IOPID}(s) = K_p + K_I/s + K_D s$ requires the determination of three optimal IOPID proportional gains (K_{P1} , K_{P2} , K_{P3}), three IOPID integral gains (K_{I1} , K_{I2} , K_{I3}) and three IOPID derivative gains (K_{D1} , K_{D2} , K_{D3}). These three proportional, integral and derivative gains of the IOPID controllers represent the constrains of the proposed optimization task. These parameters are bounded in the optimization process by certain predefined limits. The ranges of the proportional gains, integral gains and derivative gains of the three controllers are defined as following:

$$\begin{cases} K_p^{min} \leq K_{P1}, K_{P2}, K_{P3} \leq K_p^{max} \\ K_I^{min} \leq K_{I1}, K_{I2}, K_{I3} \leq K_I^{max} \\ K_D^{min} \leq K_{D1}, K_{D2}, K_{D3} \leq K_D^{max} \end{cases} \quad (43)$$

where K_p^{min} and K_p^{max} represent the minimum and maximum limits of the three proportional gains of the controllers, K_I^{min} and K_I^{max} represent the minimum and maximum limits of the three integral gains of controllers and K_D^{min} and K_D^{max} represent the minimum and maximum limits of the three derivative gains of controllers. In the selected case study, the range of the controller parameters are in between [0–200]. The control approach followed by implementing YSGA technique for tuning the controller parameters is depicted in Figure 1c.

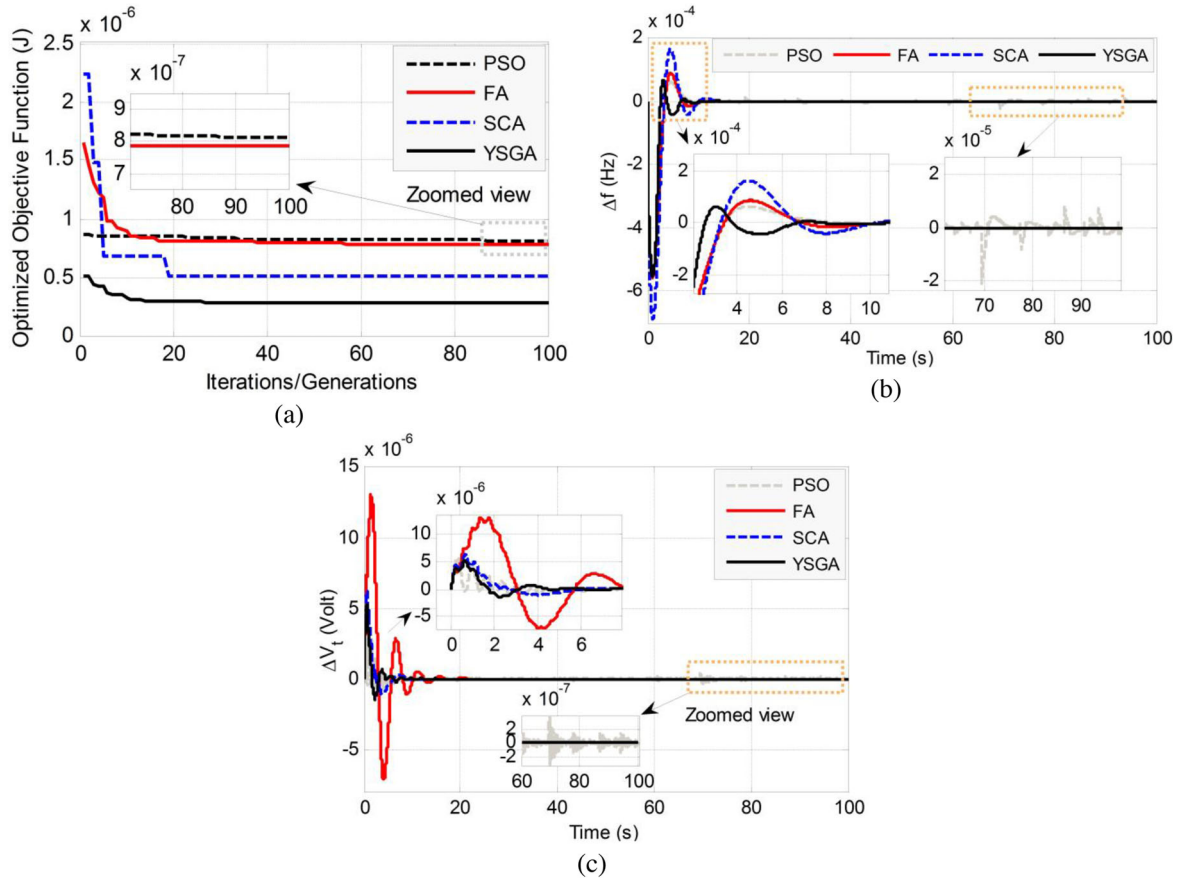


FIGURE 2 (a) Comparative convergence characteristics of different techniques, (b) assessment of Δf responses of different techniques, and (c) assessment of ΔV_t responses of different techniques.

TABLE 5 Optimum tuned controller values under different techniques

| Control technique | PSO | FA | SCA | YSGA |
|-------------------|-------|-------|-------|-------|
| K_{P1} | 40.65 | 21.04 | 12.95 | 1.002 |
| K_{I1} | 30.90 | 46.93 | 6.87 | 4.005 |
| K_{D1} | 12.47 | 36.63 | 9.82 | 49.97 |
| K_{P2} | 50.09 | 50.0 | 36.05 | 50.03 |
| K_{I2} | 50.71 | 50.19 | 43.38 | 49.99 |
| K_{D2} | 49.25 | 49.11 | 43.51 | 49.98 |
| K_{P3} | 11.03 | 3.44 | 8.15 | 6.05 |
| K_{I3} | 47.22 | 10.73 | 35.32 | 37.97 |
| K_{D3} | 2.08 | 5.14 | 3.96 | 3.98 |

TABLE 6 Statistical values assessment of several techniques (under 100 iterations)

| Measure | Worst | Best | Mean | StD | CT (s) |
|---------|-----------------------|-----------------------|-----------------------|-----------------------|--------|
| PSO | 8.59×10^{-7} | 8.13×10^{-7} | 8.28×10^{-7} | 1.57×10^{-8} | 2418 |
| FA | 1.64×10^{-6} | 7.83×10^{-7} | 8.30×10^{-7} | 1.33×10^{-7} | 2339 |
| SCA | 2.23×10^{-6} | 5.04×10^{-7} | 5.83×10^{-7} | 2.78×10^{-7} | 1987 |
| YSGA | 5.03×10^{-7} | 2.81×10^{-7} | 2.96×10^{-7} | 4.09×10^{-8} | 1804 |

TABLE 7 Comparison optimization techniques results for standard benchmark function (f_1 – f_{10}) [39]

| Functions | Computational time (s) | | | |
|-----------|------------------------|---------|----------|-----------|
| | PSO [32] | FA [33] | SCA [36] | YSGA [39] |
| f_1 | 65.65 | 59.33 | 46.21 | 28.19 |
| f_2 | 92.03 | 77.56 | 71.97 | 51.26 |
| f_3 | 102.59 | 98.78 | 88.46 | 54.74 |
| f_4 | 89.21 | 88.04 | 81.39 | 40.97 |
| f_5 | 173.01 | 177.93 | 152.84 | 124.61 |
| f_6 | 227.96 | 210.29 | 197.13 | 168.25 |
| f_7 | 284.01 | 265.09 | 230.47 | 198.32 |
| f_8 | 356.75 | 312.07 | 288.91 | 243.86 |
| f_9 | 379.38 | 344.90 | 309.73 | 287.07 |
| f_{10} | 398.62 | 371.55 | 342.69 | 305.18 |

4.2 | Assortment of controller

The selection of optimal controller is the indispensable part to extract effective system dynamics. The dynamic responses in terms of frequency and voltage under step load disturbances is analysed with PI, ID, IPD and IOPID leveraging YSGA. The

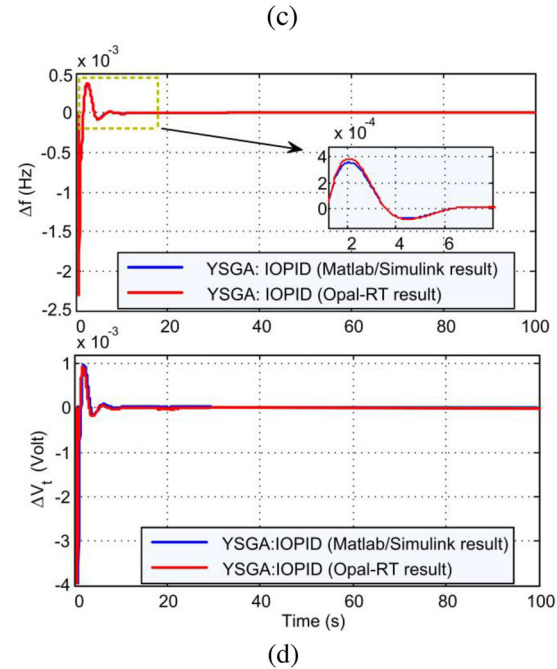
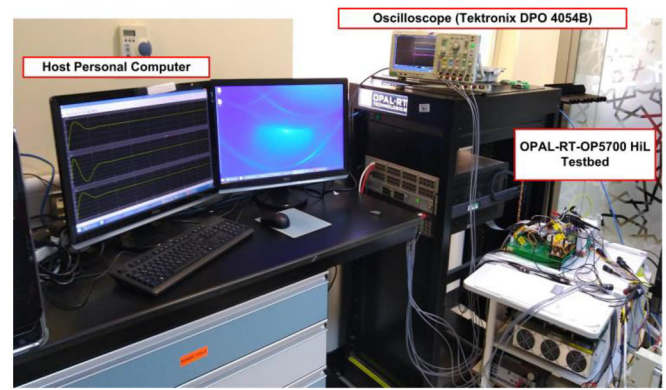
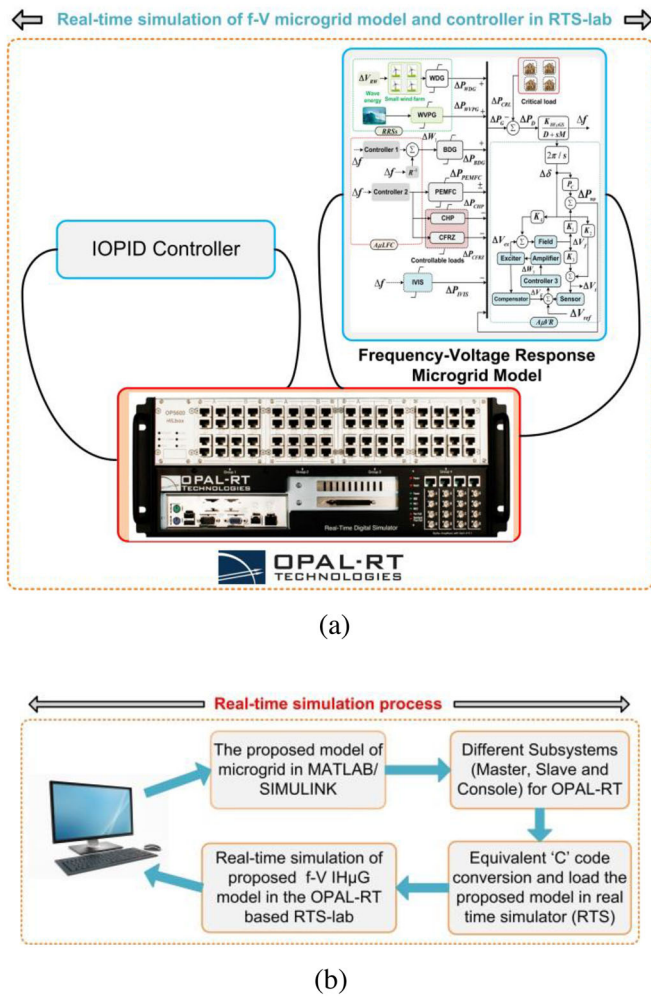


FIGURE 3 Real-time setup for experimental validation (a) Real-time simulation (using OPAL-RT) of proposed $f-V$ response model and controller. (b) Overall real-time simulation process. (c) Experimental setup of RT-Lab, (d) MATLAB/Simulink response versus Opal-RT response.

tuned values of controllers are displayed in Table 3. To select the optimum controller the decision parameters such as J , $+O_{DS}$, $-U_{DS}$ and T_{st} corresponding to the system dynamics are analysed and tabulated in Table 4. The analysed results in Tables 3 and 4 clearly interpretate the superiority of IOPID over other considered controllers. Hence the rest of assignment is utilized with IOPID controller.

4.3 | Assortment of optimization technique

To enhance the system dynamics in such an IHμG, the controller should act promptly to arrest any kind of frequency fluctuation due to occurrence of disturbance in the system. Therefore, tracking the set point by the controller demands for an effective optimization technique. The proposed assignment is considered PSO, FA, SCA and YSGA techniques and visualize the superiority of YSGA over other techniques. The comparative convergence characteristics clearly depicted the

supremacy of YSGA as illustrated in Figure 2a. The essential parameters of different techniques are listed in Appendix. The tuned controller parameters acquired by PSO, FA, SCA and YSGA techniques are displayed in Table 5. To emphasis the selection of optimum algorithmic technique a comparative statistical analysis in terms of best, worst, mean, standard deviation (StD) and computational time (CT) has been done as depicted in Table 6. In order to evaluate the computation burden, the benchmark functions [39] listed in Table 7 were tested by YSGA, SCA [36], FA [33], and PSO [32], where f_1-f_7 are unimodal benchmark functions, and f_8-f_{10} are multi-modal benchmark functions. This was done to assess the optimization performance of the considered YSGA technique. Each algorithm is tested for 100 iterations. Table 7 shows that the computing times for the suggested YSGA technique are faster than those for PSO, FA and SCA techniques for all the functions (f_1-f_{10}). Moreover, the comparative dynamic responses of frequency and voltage obtained by different algorithms are framed in Figure 2b,c. The performance assessment of different

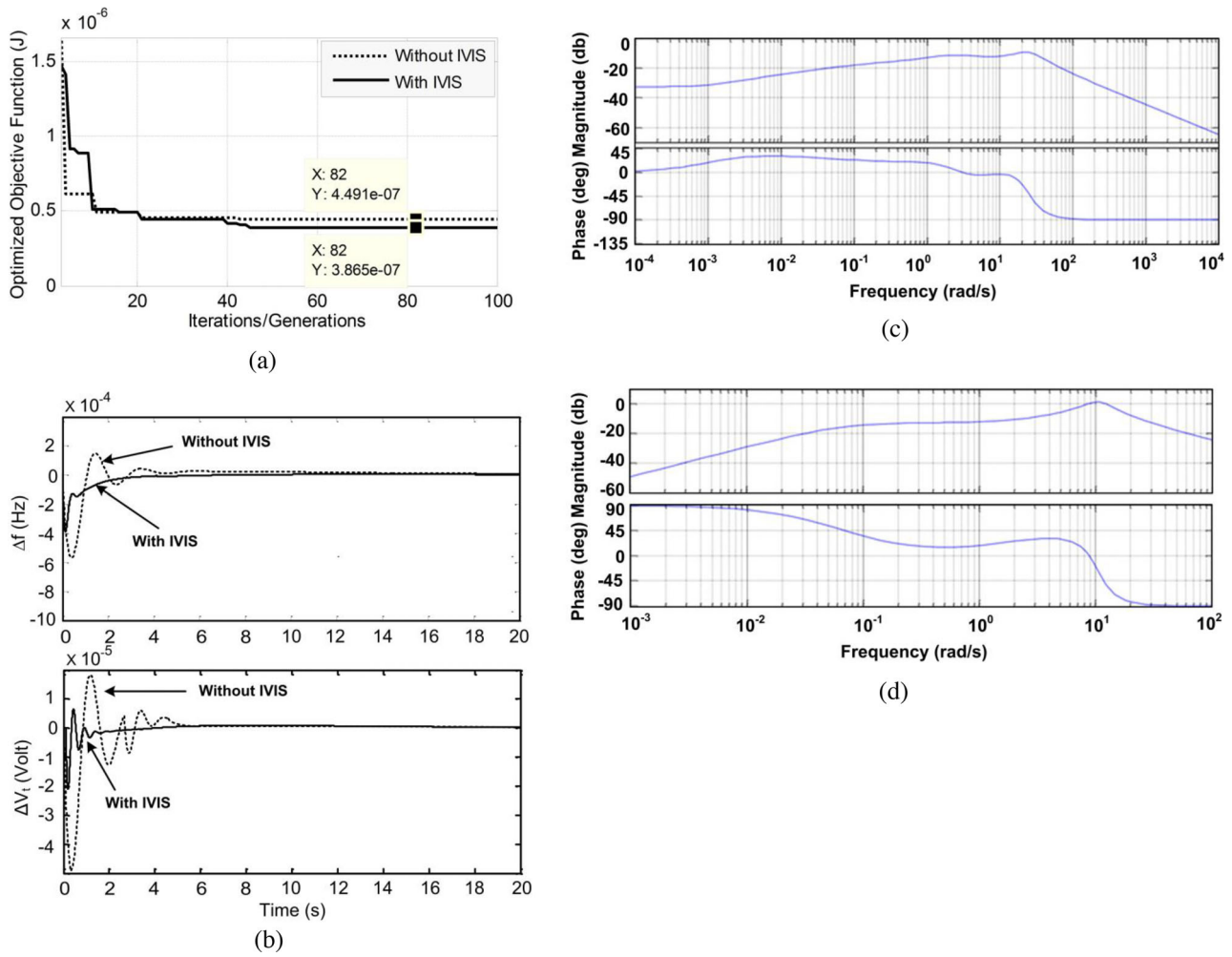


FIGURE 4 Comparative dynamic responses assessment and stability analysis under with and without IVIS scheme (a) Objective function (J) characteristics, (b) dynamic responses (Δf and ΔV_1), (c) Bode plot with IVIS scheme and (d) Bode plot without IVIS scheme.

TABLE 8 Tuned controller parameters with comparative J_{min} values

| Parameters | With IVIS | Without IVIS |
|------------|------------------------|------------------------|
| J_{min} | 3.865×10^{-7} | 4.491×10^{-7} |
| K_{P1} | 5.004 | 45.41 |
| K_{I1} | 3.087 | 47.78 |
| K_{D1} | 46.70 | 50.06 |
| K_{P2} | 49.99 | 50.0 |
| K_{I2} | 50.12 | 50.23 |
| K_{D2} | 49.98 | 49.84 |
| K_{P3} | 6.65 | 10.88 |
| K_{I3} | 49.27 | 49.80 |
| K_{D3} | 2.94 | 3.93 |

TABLE 9 Close loop system eigen values

| Eigen values |
|--|
| $-1.0031 + 0.0456i, -1.0033 - 0.0456i, -0.6342 + 0.0000i, -0.6175 + 0.0000i, -1.0000 + 0.0000i, -0.3192 + 0.0000i, -0.1801 + 0.0000i, -0.1653 + 0.0000i, -0.0856 + 0.0000i, -0.0474 + 0.0000i, -0.0441 + 0.0000i, -0.0118 + 0.0216i, -0.0119 - 0.0217i, -0.0231 + 0.0000i, -0.0121 + 0.0000i, -0.0105 + 0.0016i, -0.0105 - 0.0016i, -0.0062 + 0.0000i, -0.0101 + 0.0000i, -0.0032 + 0.0000i, -0.0022 + 0.0014i, -0.0022 - 0.0014i, -0.0021 + 0.0000i, -0.0015 + 0.0000i, -0.0008 + 0.0000i, -0.0006 + 0.0000i, -0.0003 + 0.0000i, -0.0003 + 0.0000i, -0.0001 + 0.0000i, -0.0001 + 0.0000i, -0.0001 + 0.0000i, -0.0000 + 0.0000i, -0.0000 + 0.0000i, -0.0000 + 0.0000i, -0.0000 + 0.0000i, -0.0000 + 0.0000i, -0.0000 + 0.0000i, -0.0000 + 0.0000i, -0.0000 + 0.0000i, -0.0000 + 0.0000i, -0.2400 + 0.0000i, -0.0250 + 0.0000i$ |

techniques as depicted in Figure 2 and displayed in Tables 6 and 7 justifies that YSGA technique is better than other considered techniques. Thus, the system dynamics under different case studies is established using YSGA-IOPID technique.

5 | SIMULATED TEST SYSTEM, RESULTS AND DISCUSSION

To validate the proposed control strategy, a renewable dependent IH μ G is considered as illustrated in Figure 1a and executed

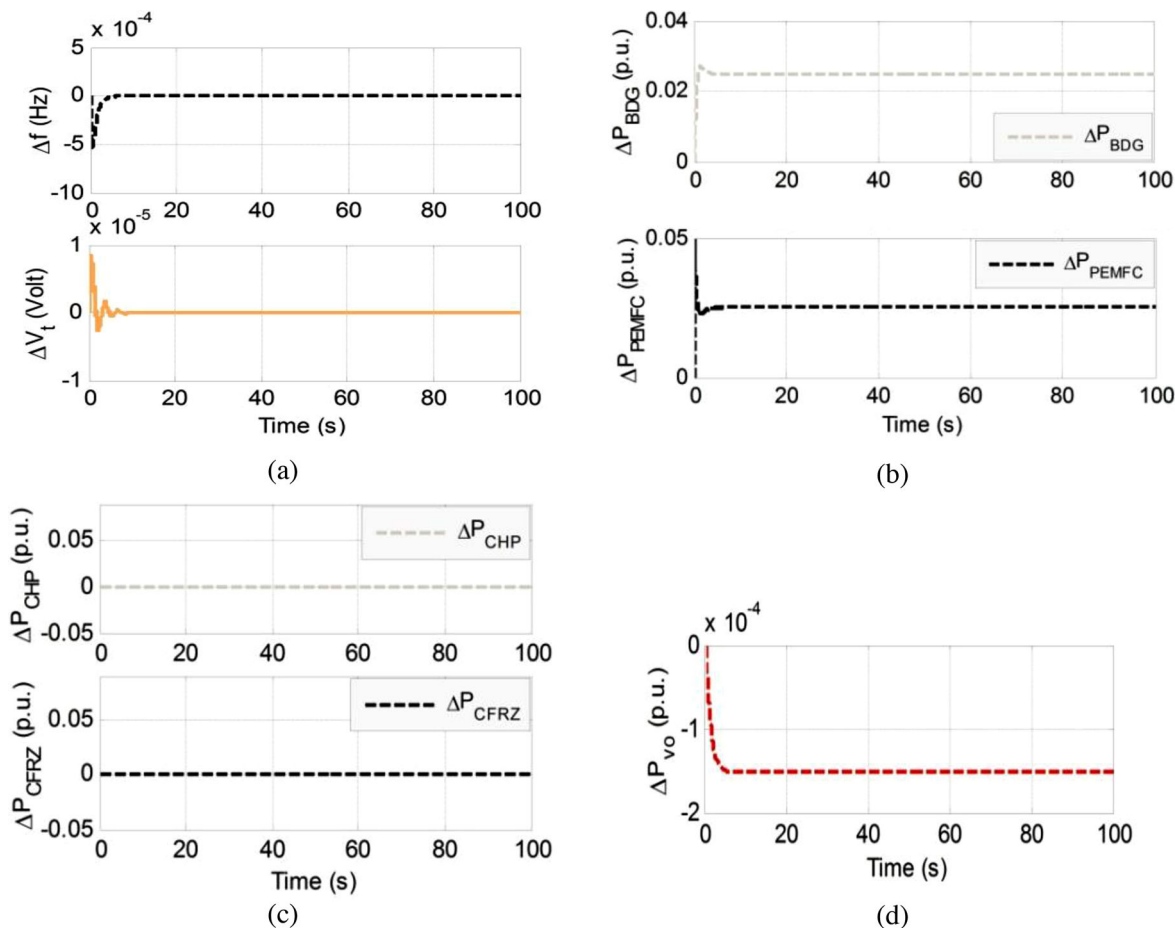


FIGURE 5 Case 1: (a) Dynamic responses (Δf and ΔV_t), (b) contributions of BDG and PEMFC, (c) contributions of CHP and CFRZ, (d) power variation of ΔP_{VR} .

under diverse circumstances leveraging MATLAB/SIMULINK R2013A environment in a computer with Core-i7-4770 CPU processor to distributed processing for faster operation. In the proposed, a real-time data is used to ensure the validation of the proposed control approach. However, for better practical realization real-time HIL simulator (under OPAL-RT lab) is utilized as shown in Figure 3a. Frequency-voltage response model is developed in MATLAB and executed in OPAL-RT OP5700 HIL system. Figure 3a presents the Host PC to integrate digital storage oscilloscope and OPAL-RT simulator. Besides, the FPGA unit is assembled inside the system with 2.6 GB its full-duplex rates. Moreover, the Simulink model has been interpreted through FPGA in the RT-Lab real-time simulator, which was done by cluster programming to make it faster and distributed execution. The data flow diagram of the assigned model under HIL test system is depicted in Figure 3b. There are three components: (i) real-time simulator for simulating frequency-voltage response IH μ G model, (ii) a command station using a PC to produce coding of the test network, (iii) a communication line to establish the connection between OPAL-RT set up and other sub-systems in the network. In fact, the RT-Lab is employed pretend delays and errors which are inherited in the off-line simulations. Figure 3c depicts an RT-Lab setup, which includes an OPAL-RT simu-

lator with PC interface that simulates the frequency response of the microgrid model from Figure 1 produced from off-line simulations. The connection between the programming host and all of the intranet's equipment is established using a router as a communication hub. To determine the difference caused by inherent delays, the outcomes of the MATLAB simulation (online) were compared to those of the OPAL-RT (RT lab), as shown in Figure 3d. Observation shows that the difference between the two results is very small, roughly matching both of them.

5.1 | Comparative system dynamics and stability analysis under with and without IVIS

The utilization of IVIS in the proposed frequency-voltage response model is a novel approach. In this assignment, IVIS is leveraged to observe the effect in the system dynamics as well as to enhance the dynamic responses (frequency and voltage) when subject to various disturbances conditions. A comparative assessment is conducted with and without the IVIS scheme. Results validate the superiority of the IVIS scheme in power sharing along with transient issues. The optimized convergence response is established in Figure 4a, whereas the system

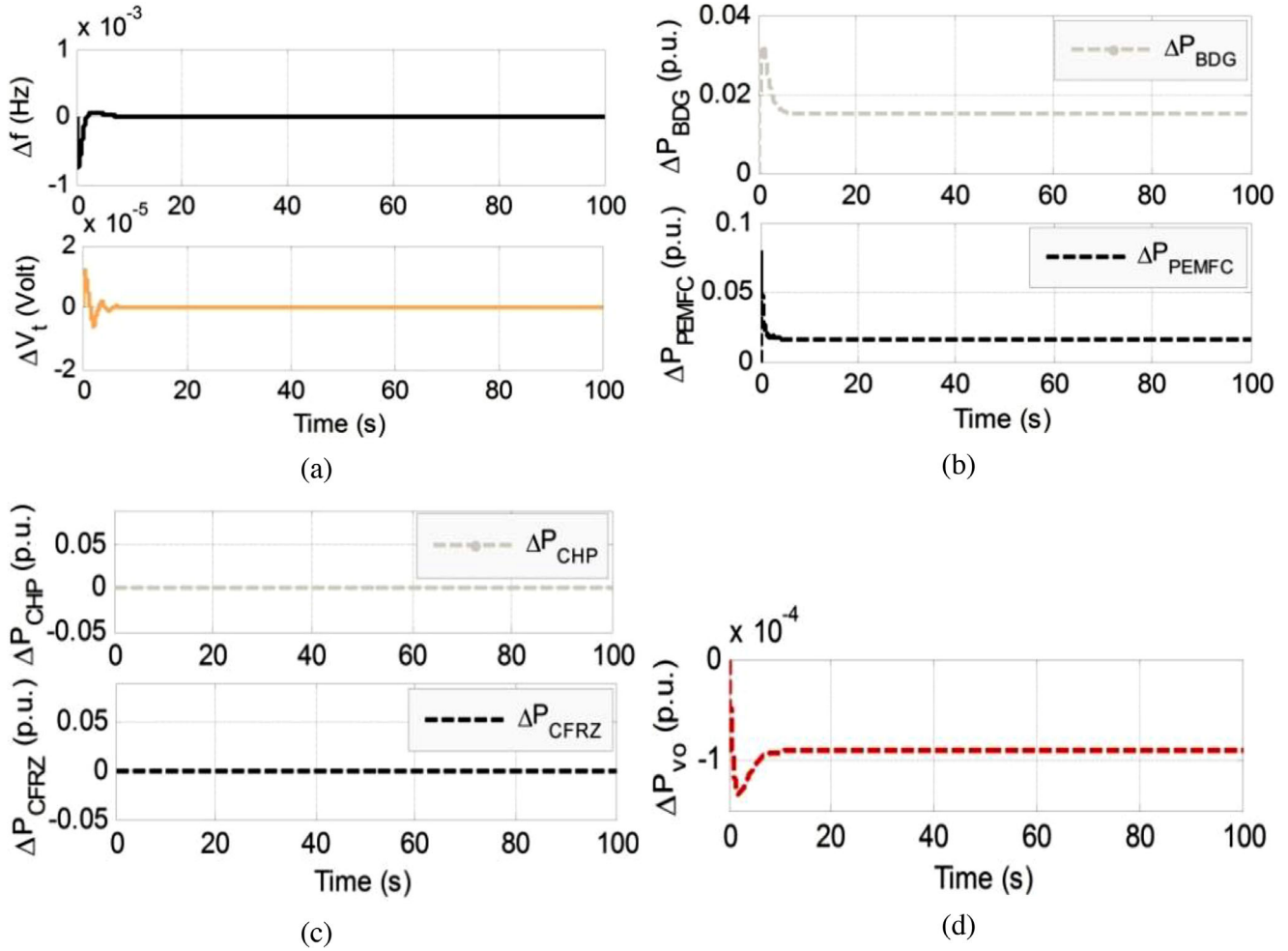


FIGURE 6 Case 2: (a) Dynamic responses (Δf and ΔV_t), (b) contributions of BDG and PEMFC, (c) contributions of CHP and CFRZ, (d) power variation of ΔP_{vo} .

dynamics (Δf and ΔV_t) considering IVIS against without IVIS is depicted in Figure 4b. The tuned controller parameters with J_{min} values are displayed in Table 8. In order to demonstrate good performance, stability analysis of closed loop is also assessed via the eigenvalues and bode plots. The eigenvalues and bode plots, obtained with IVIS being in the loop, are presented in Table 9 and Figure 4c, respectively. All eigenvalues lying to the left of ' $j\omega$ ' axis clearly establish system stability and the fact that most of those having fairly large negative real part is indicative of the sufficient stability margin the system has. Besides, the small imaginary parts of the eigenvalues ensure that the system dynamics settle faster and smoother. Further, the examination of bode plots in Figure 4c brings out the stability aspect in terms of positive gain and phase margins, thus ascertaining that the consideration of IVIS is stable. For relative stability assessment of the proposed control scheme, the bode plots are also obtained without IVIS scheme and are shown in Figure 4d in which case also the system is stable, however with slightly delayed characteristics. Hence, the rest of the assignment is followed by IVIS integrated control strategy with the same optimal controllers' parameters.

5.2 | Dynamic responses of system under different disturbances

The studied microgrid's frequency and voltage dynamics are investigated under different disturbances case conditions using IVIS stratagem integrated IOPID optimized YSGA technique.

5.2.1 | Case 1: Non-availability of all RRs

In this scenario, it is assumed that due to some maintenance problem all RRs are unavailable. Hence, the power contributions from all the RRs are zero. A constant 5% change in load (ΔP_{CRL}) disturbances is considered for the entire 100 s run time. Due to the non-availability of RRs the coordinated power sharing of biodiesel generation (ΔP_{BDG}), proton exchange based fuel cell (ΔP_{PEMFC}) plays a vital role maintain the deficit load demand as depicted in Figure 5. The system dynamics (Δf and ΔV_t) along with the sharing of power of other subsystems are framed in Figure 5, whereas the coordinated ΔP_{vo} is depicted in Figure 5d.

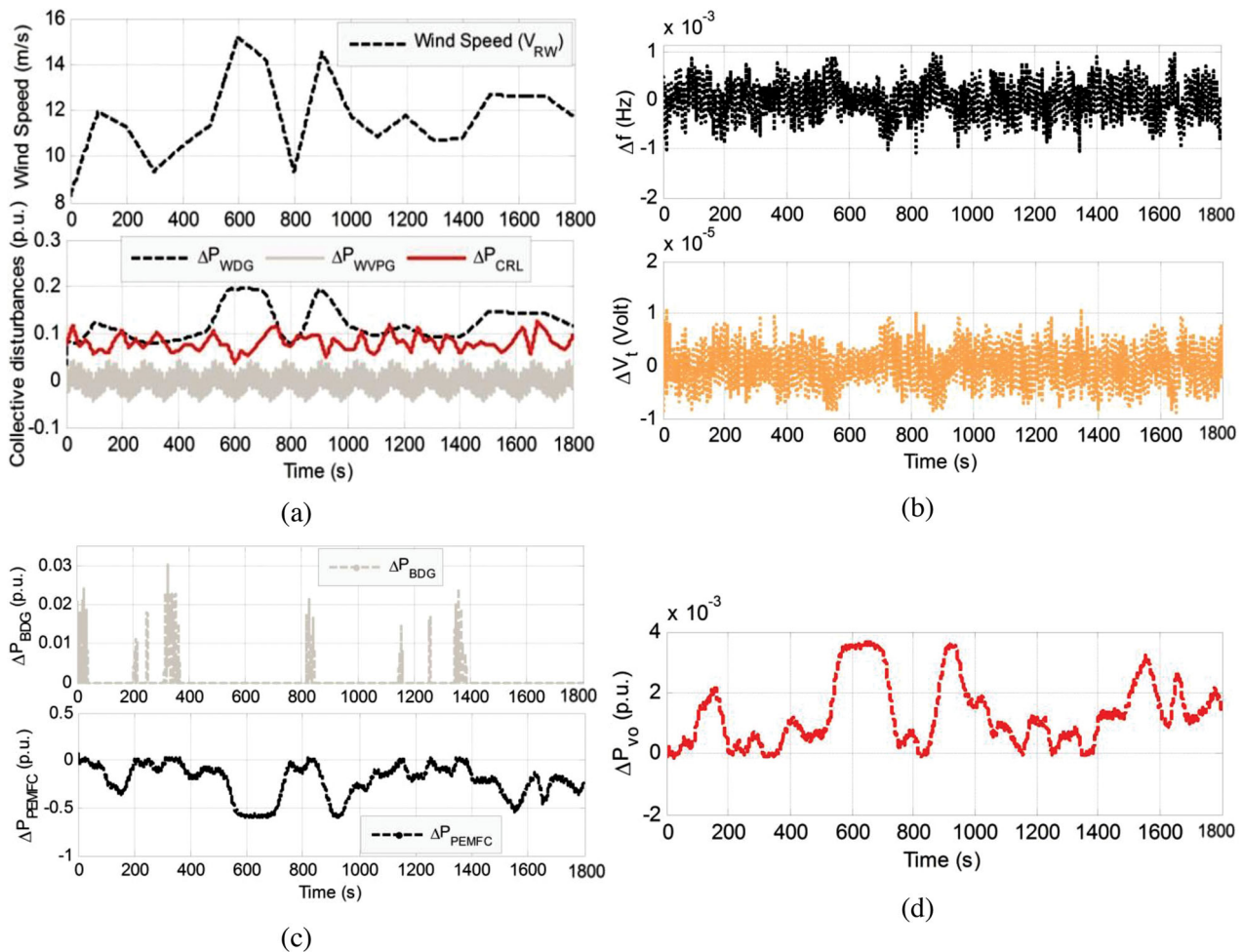


FIGURE 7 Case 3: (a) Real-time wind velocity with multiple disturbances (b) Dynamic responses (Δf and ΔV_t), (c) contributions of BDG and PEMFC, (d) power variation of ΔP_{vo} .

5.2.2 | Case 2: Availability of all RRs

This case is presumed with considering a nominal climatic scenario consisting of available change in WDG (ΔP_{WDG}) of 3% and change in WVPG (ΔP_{WVPG}) of 2% to supply the demanded 8% constant load (ΔP_{CRL}). The biodiesel generation (ΔP_{BDG}), photon exchange-based fuel cell (ΔP_{PEMFC}) shared their changeable power to meet the excess load demand as framed in Figure 6. Moreover, the contributions of controllable loads (ΔP_{CHP} and ΔP_{CFRZ}) are displayed in Figure 6.

The dynamic responses (Δf and ΔV_t) corresponding to above mentioned prescribed case are framed in Figure 6. The regulated ΔP_{vo} is displayed in Figure 6d.

5.2.3 | Case 3: Real-time random disturbance of WDG and other collective non-linear variation of generation-load

This subheading established the dynamic responses against real recorded wind speed (V_{RW}) as collected from NIWE, Govt. of India [45] as depicted in Appendix. An average value of

8% of the non-linear patterned critical load (ΔP_{CRL}) is leveraged as framed in Figure 7a. However, considered non-linear sinusoidal patterned wave power generation is formulated by Equation (44).

$$\Delta P_{WVPG} = \left\{ \begin{array}{l} 0.013 \sin(0.05t) + 0.02 \sin(0.05t) \\ + 0.04 \sin(1.2t) \end{array} \right\} \quad (44)$$

The system dynamics in terms of frequency and voltage of the projected IH μ G in this case study are plotted in Figure 7b. To maintain the dynamic responses within the allowable range the sharing of change in power of other subsystems are depicted in Figure 7c. The coordinated ΔP_{vo} is depicted in Figure 7d.

5.2.4 | Case 4: Sensitivity assessment of the proposed control scheme under collective uncertainties and parametric variations

To establish the sturdiness of the proposed control mechanism under YSGA technique tuned IOPID controller considering

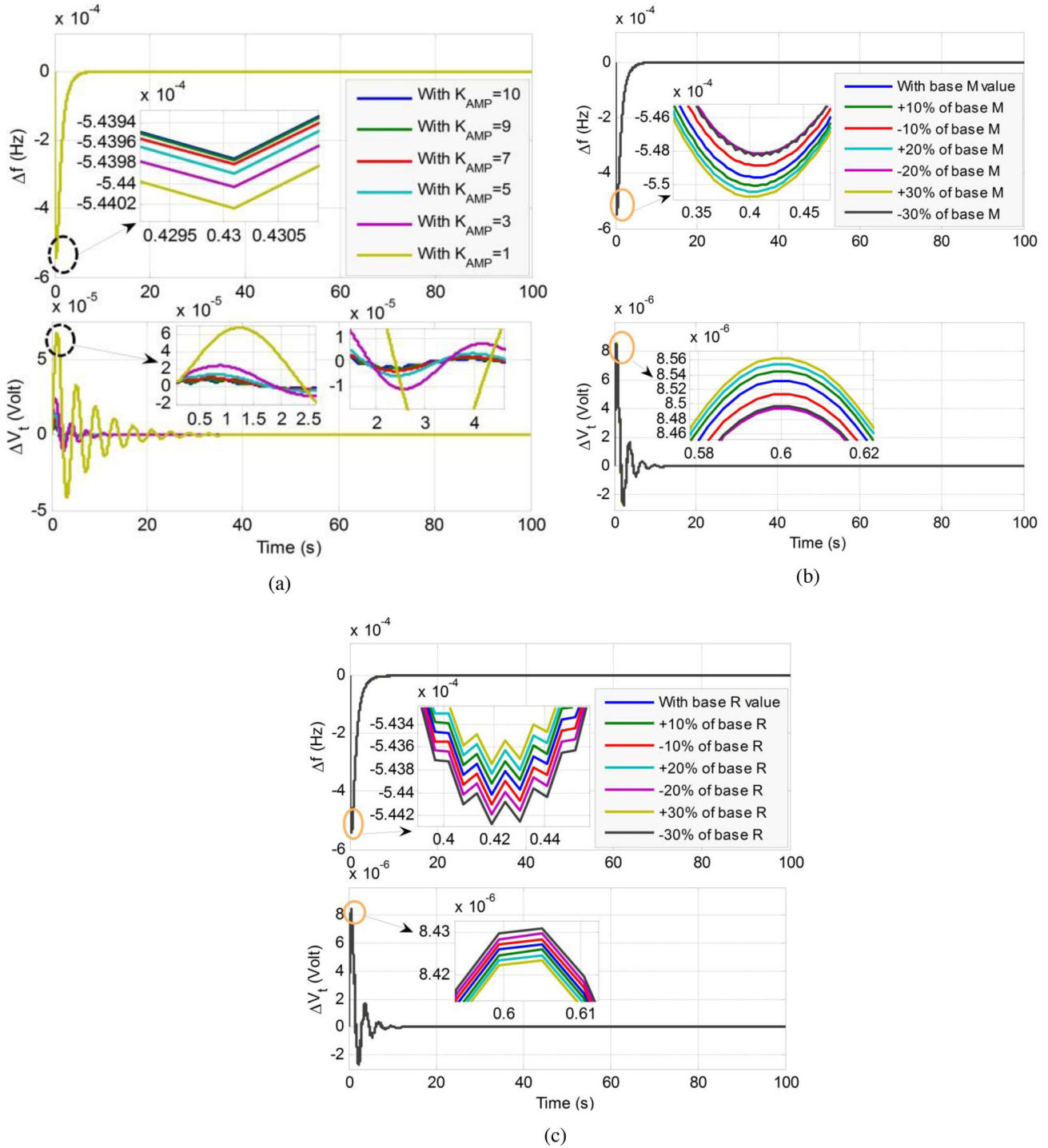


FIGURE 8 System dynamics assessment pertaining to base operating case and different parametric (i.e. change of K_{AMP} , $\pm 30\%$ of M and R) varied conditions (a) Dynamic responses (Δf and ΔV_t), (b) dynamic responses (Δf and ΔV_t) and (c) dynamic responses (Δf and ΔV_t).

IVIS scheme, a base condition of a constant variations (ΔP_{WDG} , ΔP_{WVPG} , ΔP_{CRL}) of 0%, 0% and 40% is considered at $t = 0$ s onwards as a case scenario. To validate the robustness of IOPID controller corresponding to the above said base scenario an effective parametric variations of proposed IH μ GS will occurs which deviates the base conditions values of $\pm 30\%$ loading condition (ΔP_{CRL}), $\pm 30\%$ microgrid inertia constant (M), microgrid droop coefficient (R) and amplifier gain

(K_{AMP}) to assess the sensitivity analysis. The corresponding system dynamics under such parametric variations are framed in Figures 8 and 9 respectively. It could be noted that, the imposing $\pm 30\%$ change in R and M leads to slight deviation (almost overlapping) as depicted in Figure 8. However, the wide changes of (up to $\pm 30\%$) of system loading condition the system dynamics framed in Figure 9 is not fluctuate that much from its base condition.

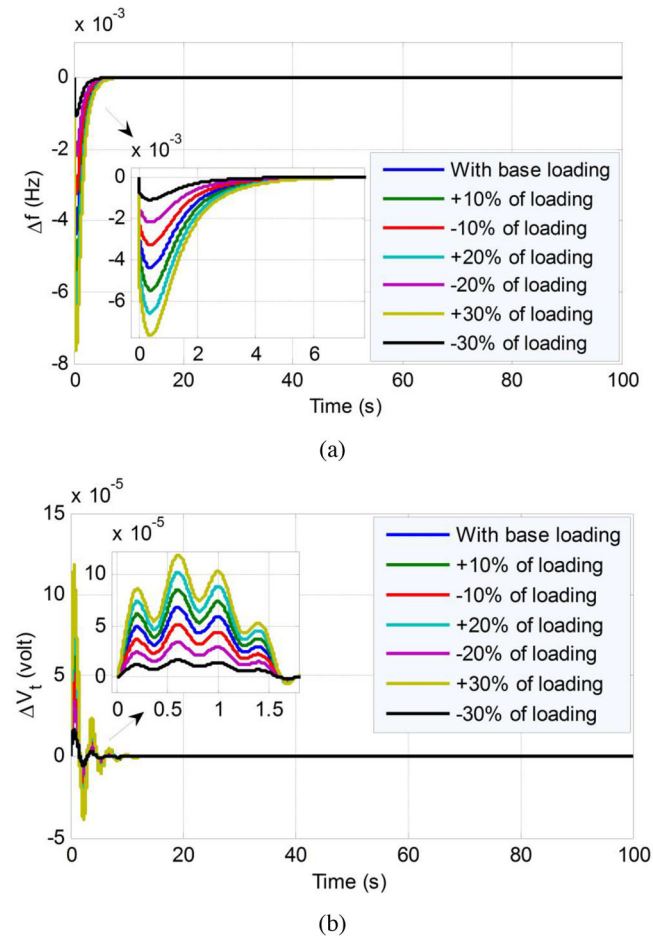


FIGURE 9 System dynamics assessment pertaining to base case and $\pm 30\%$ loading pattern changed condition (a) Dynamic responses in terms of Δf and (b) dynamic responses in terms of ΔV_t .

The sturdiness in terms of performance indicators ($+O_{vs}$, $-U_{vs}$, and T_{st}) for changing the loading condition ($\pm 10\%$ to $\pm 30\%$) is tabulated in Table 10. The dynamic responses reveals that the IVIS enabled proposed control strategy is robust enough without resetting the controllers parameters.

6 | CONCLUSION

This article investigates a novel improved virtual inertia support (IVIS) scheme for coordinated frequency and voltage regula-

tion during contingencies under proposed diversified IH μ GS. Said power system includes different renewable energy-based generators such as WDG, WVPG, BDG, BGPG, PEMFC, and controllable loads. Another contribution of this work is a frequency-voltage (f - V) response model is developed for PEMFC for the first time. A maiden effort has been made to assess the dynamic responses of using IOPID controller in the proposed f - V response model. The application of a recently developed technique named YSGA is leveraged to accomplish optimal control parameters and demonstrated by framing the system dynamics of IVIS enabled proposed IH μ GS, which is a unique work. Several comparative studies have been pondered and assessed with respect to PI/ID/IPD controllers and algorithmic techniques under various operating scenarios.

Results reveal that the YSGA-IOPID controller is superior in terms of decision indicators ($+O_{vs}$, $-U_{vs}$ and T_{st}) and J_{FOD} values. The comparative responses evaluation of the proposed model with/without IVIS scheme indicates that the proposed IOPID based IVIS approach could stabilize the frequency and actual voltage deviation more effectively. The sensitivity study of the YSGA-IOPID controller, considering the parametric variation of R , M , K_{AMP} , and loading, demonstrated that the proposed IVIS is robust and achieves stable operation in studied IH μ GS. Real-time validation of the control approach OPAL-RT based Hardware-in-the-Loop (HIL) simulation is utilized to study real-time responses.

The proposed IVIS is valuable in stabilizing voltage and frequency in renewable energy-dominated microgrids. Extensive studies comparing different controllers and optimization algorithms will help researchers in designing more stable and effective systems. All of these will expedite the transition to renewable energy-based microgrids.

AUTHOR CONTRIBUTIONS

Abdul Latif: Conceptualization, Formal analysis, Investigation, Methodology, Software, Validation, Writing - original draft, Writing - review & editing. S. M. Suhail Hussain: Conceptualization, Formal analysis, Investigation, Methodology, Validation, Writing - review & editing. Atif Iqbal: Conceptualization, Funding acquisition, Project administration, Supervision, Writing - review & editing. D. C. Das: Conceptualization, Project administration, Resources, Supervision, Validation, Writing - review & editing. Taha Selim Ustun: Conceptualization, Project administration, Supervision, Writing - review & editing. Ahmed Aldurra: Conceptualization, Project administration, Supervision, Writing - review & editing.

TABLE 10 $+O_{vs}$, $-U_{vs}$ and T_{st} under change in operating loading magnitude

| Obtained from [Figure 9a,b] | | % change of loading | | | | | |
|-----------------------------|----------------------------|---------------------|-------|-------|-------|-------|-------|
| | | +10% | -10% | +20% | -20% | +30% | -30% |
| Δf | $-U_{vs} (\times 10^{-3})$ | 5.437 | 3.267 | 6.534 | 2.181 | 7.597 | 1.091 |
| | $T_{St} (s)$ | 4.017 | 3.59 | 4.317 | 3.552 | 5.110 | 3.194 |
| ΔV_t | $+O_{vs} (\times 10^{-3})$ | 0.084 | 0.050 | 0.101 | 0.033 | 0.118 | 0.016 |
| | $T_{St} (s)$ | 14.94 | 12.99 | 15.19 | 12.17 | 15.43 | 11.58 |

ACKNOWLEDGEMENTS

The APC for this paper was funded by Qatar National Library (QNL), Doha, Qatar. This work was supported in part by Khalifa University under award no. KAU-KU-2021-01. The statements made herein are solely the responsibility of the authors.



CONFLICT OF INTEREST STATEMENT

The authors declare no conflicts of interest.

DATA AVAILABILITY STATEMENT

The data that support the findings of this study are openly available at http://niwe.res.in:8080/NIWE_WRA_DATA/DataTable_D4.jsf, reference number [34].

ORCID

S. M. Subail Hussain  <https://orcid.org/0000-0002-7779-8140>
Atif Iqbal  <https://orcid.org/0000-0002-6932-4367>

REFERENCES

- Said, S.M., Aly, M., Hartmann, B., Alharbi, A.G., Ahmed, E.M.: Smesbased fuzzy logic approach for enhancing the reliability of microgrids equipped with pv generators. *IEEE Access* 7, 92059–92069 (2019)
- Aly, M., Ahmed, E.M., Shoyama, M.: Thermal and reliability assessment for wind energy systems with dstatcom functionality in resilient microgrids. *IEEE Trans. Sustainable Energy* 8(3), 953–965 (2017)
- Guo, C., Wang, X., Zheng, Y., Zhang, F.: Optimal energy management of multi-microgrids connected to distribution system based on deep reinforcement learning. *Int. J. Electr. Power Energy Syst.* 131, 107048 (2021)
- Kerdphol, T., Rahman, F.S., Mitani, Y., Watanabe, M., Küfeoğlu, S.: Robust virtual inertia control of an islanded microgrid considering high penetration of renewable energy. *IEEE Access* 6, 625–636 (2017)
- Zhao, H., Yang, Q., Zeng, H.: Multi-loop virtual synchronous generator control of inverter-based dgs under microgrid dynamics. *IET Gener. Transm. Distrib.* 11(3), 795–803 (2017)
- Das, D.C., Roy, A.K., Sinha, N.: GA based frequency controller for solar thermal–diesel–wind hybrid energy generation/energy storage system. *Int. J. Electr. Power Energy Syst.* 43(1), 262–279 (2012)
- Li, J., Xiong, R., Yang, Q., Liang, F., Zhang, M., Yuan, W.: Design/test of a hybrid energy storage system for primary frequency control using a dynamic droop method in an isolated microgrid power system. *Appl. Energy* 201, 257–269 (2017)
- Gheisarnejad, M., Hassan Khooban, M.: Secondary load frequency control for multi-microgrids: HiL real-time simulation. *Soft Comput.* 23(14), 5785–5798 (2019)
- Hussain, I., Das, D.C., Sinha, N.: Reactive power performance analysis of dish–Stirling solar thermal–diesel hybrid energy system. *IET Renewable Power Gener.* 11(6), 750–762 (2017)
- Zhu, X., Xia, M., Chiang, H.D.: Coordinated sectional droop charging control for EV aggregator enhancing frequency stability of microgrid with high penetration of renewable energy sources. *Appl. Energy* 210, 936–943, (2018)
- Lakshmanan, V., Marinelli, M., Hu, J., Bindner, H.W.: Provision of secondary frequency control via demand response activation on thermostatically controlled loads: Solutions and experiences from Denmark. *Appl. Energy* 173, 470–480 (2016)
- Gupta, A., Chauhan, A., Khanna, R.: Design of AVR and ALFC for single area power system including damping control. In: *2014 Recent Advances in Engineering and Computational Sciences (RAECS)*. Chandigarh, pp. 1–5 (2014)
- Othman, A.M., El-Fergany, A.A.: Design of robust model predictive controllers for frequency and voltage loops of interconnected power systems including wind farm and energy storage system. *IET Gener. Transm. Distrib.* 12(19), 4276–4283 (2018)
- Rajbongshi, R., Saikia, L.C.: Combined control of voltage and frequency of multi-area multisource system incorporating solar thermal power plant using LSA optimised classical controllers. *IET Gener. Transm. Distrib.* 11(10), 2489–2498 (2017)
- Bevrani, H., Ise, T., Miura, Y.: Virtual synchronous generators: A survey and new perspective. *Int. J. Electr. Power Energy Syst.* 54, 244–254 (2014)
- Rakhshani, E., Remon, D., Cantarellas, A.M., Garcia, J.M., Rodriguez, P.: Virtual synchronous power strategy for multiple HVDC interconnections of multi-area AGC power systems. *IEEE Trans. Power Syst.* 32(3), 1665–1677 (2017)
- Rakhshani, E., Remon, D., Cantarellas, A.M., Rodriguez, P.: Analysis of derivative control based virtual inertia in multi-area high-voltage direct current interconnected power systems. *IET Gener. Transm. Distrib.* 10(6), 1458–1469 (2016)
- Rakhshani, E., Rodriguez, P.: Inertia emulation in AC/DC interconnected power systems using derivative technique considering frequency measurement effects. *IEEE Trans. Power Syst.* 32(5), 3338–3351 (2017)
- Kerdphol, T., Fathin, S.R., Watanabe, M., Mitani, Y.: Robust virtual inertia control of a low inertia microgrid considering frequency measurement effects. *IEEE Access* 7, 57550–57560 (2019)
- Fini, M.H., Golshan, M.E.H.: Determining optimal virtual inertia and frequency control parameters to preserve the frequency stability in islanded microgrids with high penetration of renewables. *Electr. Power Syst. Res.* 154, 13–22 (2018)
- Alhejaj, S.M., Gonzalez-Longatt, F.M.: Impact of inertia emulation control of grid-scale BESS on power system frequency response. In: *Proceedings of International Conference on Students on Applied Engineering (ICSAE)*. Newcastle, UK, pp. 254–258 (2016)
- Kerdphol, T., Rahman, F.S., Mitani, Y., Hongesombut, K., Küfeoğlu, S.: Virtual inertia control-based model predictive control for microgrid frequency stabilization considering high renewable energy integration. *Sustainability* 9(5), 773 (2017)
- Kerdphol, T., Rahman, F.S., Mitani, Y.: Virtual inertia control application to enhance frequency stability of interconnected power systems with high renewable energy penetration. *Energies* 11(4), 981–997 (2018)
- Kerdphol, T., Rahman, F.S., Mitani, Y., Watanabe, M., Küfeoğlu, S.: Robust virtual inertia control of an islanded microgrid considering high penetration of renewable energy. *IEEE Access* 6, 625–636 (2017)
- Sockeel, N., Gafford, J., Papari, B., Mazzola, M.: Virtual inertia emulator-based model predictive control for grid frequency regulation considering high penetration of inverter-based energy storage system. *IEEE Trans. Sustainable Energy* 11(4), 2932–2939 (2020)
- Fang, J., Zhang, R., Li, H., Tang, Y.: Frequency derivativebased inertia enhancement by grid-connected power converters with a frequency-locked-loop. *IEEE Trans. Smart Grid.* 10, 4918–4927 (2019)
- Nogami, S., Yokoyama, A., Daibu, T., Hono, Y.: Virtual synchronous generator model control of PV for improving transient stability and damping in a large-scale power system. *IEEJ Trans. Power Energy* 138(8), 716–723 (2019)
- Shintai, T., Miura, Y., Ise, T.: Oscillation damping of a distributed generator using a virtual synchronous generator. *IEEE Trans. Power Delivery* 29(2), 668–676 (2014)
- Aftab, M.A., Hussain, S.M.S., Latif, A., Das, D.C., Ustun, T.S.: IEC 61850 communication based dual stage load frequency controller for isolated hybrid microgrid. *Int. J. Electr. Power Energy Syst.* 130, 106909 (2021)
- Phurailatpam, C., Rather, Z.H., Bahrani, B., Doolla, S.: Measurement based estimation of inertia in AC microgrids. *IEEE Trans. Sustainable Energy* 11(3), 1975–1984 (2020)
- El-Fergany, A.A., El-Hameed, M.A.: Efficient frequency controllers for autonomous two-area hybrid microgrid system using social-spider optimiser. *IET Gener. Transm. Distrib.* 11(3), 637–648 (2017)
- Latif, A., Das, D.C., Ranjan, S., Barik, A.K.: Comparative performance evaluation of WCA-optimised non-integer controller employed with WPG–DSPG–PHEV based isolated two-area interconnected microgrid system. *IET Renewable Power Gener.* 13(5), 725–736 (2019)
- Latif, A., Das, D.C., Barik, A.K., Ranjan, S.: Illustration of demand response supported co-ordinated system performance evaluation of YSGA optimized dual stage PIFOD-(1+ pi) controller employed with

- wind-tidal-biodiesel based independent two-area interconnected microgrid system. IET Renewable Power Gener. 14(6), 1074–1086 (2020)
34. Pahasa, J., Ngamroo, I.: Coordinated control of wind turbine blade pitch angle and PHEVs using MPCs for load frequency control of microgrid. IEEE Syst. J. 10, 97–105 (2016)
 35. Latif, A., Hussain, S.M.S., Das, D.C., Ustun, T.S.: State-of-the-art of controllers and soft computing techniques for regulated load frequency management of single/multi-area traditional and renewable energy based power systems. Appl. Energy 266, 114858 (2020)
 36. Tasnin, W., Saikia, L.C.: Maiden application of a sine–cosine algorithm optimised FO cascade controller in automatic generation control of multi-area thermal system incorporating dish–Stirling solar and geothermal power plants. IET Renewable Power Gener. 12, 585–597 (2018)
 37. Singh, K., Amir, M., Ahmad, F., Khan, M.A.: An integral tilt derivative control strategy for frequency control in multimicrogrid system. IEEE Syst. J. 15(1), 1477–1488 (2021)
 38. Latif, A., Hussain, S.M.S., Das, D.C., Ustun, T.S.: Double stage controller optimization for load frequency stabilization in hybrid wind–ocean wave energy based maritime microgrid system. Appl. Energy 282, 116171 (2021)
 39. Zaldivar, D., et al.: A novel bio-inspired optimization model based on yellow saddle goatfish behavior. BioSystems 174, 1–21 (2018).
 40. Lee, D.J., Wang, L.: Small-signal stability analysis of an autonomous hybrid renewable energy power generation/energy storage system part I: Time-domain simulations. IEEE Trans. Energy Convers. 23, 311–320 (2008)
 41. Hasanien, M.H.: Whale optimisation algorithm for automatic generation control of interconnected modern power systems including renewable energy sources. IET Gener. Transm. Distrib. 12, 607–614 (2018)
 42. Taghizadeh, M., Mardaneh, M., Sadeghi, M.S.: Frequency control of a new topology in proton exchange membrane fuel cell/wind turbine/photovoltaic/ultra-capacitor/battery energy storage system based isolated networks by a novel intelligent controller. J. Renewable Sustainable Energy 6(5), 053121 (2014)
 43. Latif, A., Das, D.C., Barik, A.K., Ranjan, S.: Maiden co-ordinated load frequency control strategy for ST-AWEC-GEC-BDDG based independent three-area interconnected microgrid system with the combined effect of diverse energy storage and DC link using BOA optimized PFOID controller. IET Renewable Power Gener. 13, 2634–2646 (2019)
 44. Anderson, P.M., Fouad, A.A.: Effect of stability on excitation system. In: Power System Control and Stability, 2nd ed. pp. 309–366. John Wiley & Sons, Hoboken, NJ (2008)
 45. Wind Speed Data: http://niwe.res.in:8080/NIWE_WRA_DATA/DataTable_D4.jsf

How to cite this article: Latif, A., Suhail Hussain, S.M., Iqbal, A., Das, D.C., Ustun, T.S., Al-Durra, A.: Concurrent frequency–voltage stabilization for hybrid microgrid with virtual inertia support. IET Renew. Power Gener. 1–19 (2023).
<https://doi.org/10.1049/rpg2.12729>

APPENDIX

WDG [45]: Date of recorded data: 01 July, 2016; Minimum velocity of wind: 7.4804 m/s; Maximum velocity of wind: 14.08 m/s; Average velocity of wind: 10.922 m/s; SD: 1.1895.

PSO [32]: No of population: 50; Maximum iteration (Itr_{Max}): 100, Maximum weight factor (W_{max}): 0.9, Minimum weight factor (W_{min}): 0.1; Acceleration factors (C1 and C2): 2.

FA [33]: No of fireflies (n): 50; Light absorption factor (γ): 0.5; Attractiveness factor (β): 0.2; Scaling factor (s): 0.2; Maximum iteration (Itr_{Max}): 100.

SCA [36]: No of search agents (n): 50; Maximum iteration (Itr_{Max}): 100; Search co-efficient (α) = 2.

YSGA [39]: No of search agents (n): 50; No. of clusters (K) = 4; Overexploitation parameters (λ) = 10; Spiral direction constraints (b) = 1; Random number (ρ) = [a , 1]; Maximum iteration (Itr_{Max}): 100.